Vibrations of mechanical systems undergoing regularized unilateral contact conditions through the wavelet balance method

Simon Jones, Mathias Legrand

Vibrations of mechanical systems undergoing regularized unilateral contact conditions through the wavelet balance method

Simon Jones[1]*, Mathias Legrand[2]

Abstract

The method of weighted residuals can efficiently enforce time-periodic solutions of flexible structures experiencing unilateral contact. The Harmonic Balance Method (HBM) based on Fourier expansion of the sought solution is a common formulation, though wavelet bases that can sparsely define nonsmooth solutions may be superior. This hypothesis is investigated using an axially vibrating rod with unilateral contact conditions. A distributional formulation in time is introduced allowing $L^2(\mathbb{S}^1)^N$ trial functions to approximate the second-order equations. The mixed wavelet Petrov-Galerkin solutions are found to yield consistent or better results than HBM, with similar convergence rates and seemingly more accurate contact force prediction.

Keywords

wavelet analysis — Petrov-Galerkin method — weak formulation — unilateral contact conditions — nonsmooth dynamics

[1]Department of Mechanical Engineering, B108B Moench Hall, Rose-Hulman Institute of Technology, 5500 Wabash Avenue, Terre Haute, Indiana 47803-3999
[2]Department of Mechanical Engineering, McGill University, Macdonald Engineering Building, Room 270, 817 Sherbrooke Street West, Montreal, Quebec H3A 0C3
***Corresponding author**: jones5@rose-hulman.edu, (+001) 812.877.8926

1. Introduction

Efficiently predicting the vibratory responses of flexible structures which experience unilateral contact is becoming of high engineering importance. This type of response is increasingly common in industrial applications due to implementation of light materials and thin designs involving larger displacements together with tighter operating clearances between components. For example, consider aircraft engines where slender, twisted blades rotate at high rotational velocity within stationary casings where minimal clearance is desirable for turbine energy efficiency. Simulating contact between the blades and casing is not a trivial exercise since unilateral contact is usually described by inequalities and complementary conditions [42]. In the time domain, structural displacements and velocities which satisfy these non-penetration Signorini conditions are known to respectively feature absolute continuity and bounded variation only [34]. This implies displacements are not necessarily differentiable everywhere in the defined domain and velocities may exhibit jumps; these types of problems are generally referred to as nonsmooth. Broadly speaking, existence of solutions is still an open problem and intense research is devoted to the derivation of efficient time-stepping solution methods [1, 22].

This class of unilateral problems can also be approached using periodic vibration theory. This allows the original initial-value formulations to be transformed into partial differential equations periodic in time [20]. In structural mechanics, two families of numerical techniques can efficiently describe approximated periodic solutions in time while maintaining computational efficiency. The first is commonly known as the shooting method which consists of finding the initial conditions that realize a periodic motion; for free responses the period of the motion can also be an unknown. The overall approach relies on time integration of the governing equations over one period using a nonlinear solver which iterates on the initial conditions, and possibly the period. The second technique is based on weighted residual formulations, which are of interest in the current investigation. This method involves approximating the solution using a set of time-dependent basis functions, called trial functions, and enforcing the respective residual error to be orthogonal to an independent set of weighting functions [19, 31]. The orthogonality is enforced using an inner product in the sense of a scalar product adequately defined on a functional Hilbert space.

Unlike the shooting method which can become numerically sensitive to possible jumps in the velocity field, weighted residual techniques directly enforce the periodicity conditions while the remaining unilateral contact constraints and governing local equations of motion are satisfied in a weak integral sense [40, 13]. It is worth noting that the well-known Harmonic Balance Method (HBM) is a weighted residual approach where both the trial and weighting functions are identical Fourier series. The main goal of the current work is to explore relevant basis functions whose order of smoothness can be adapted to a particular system to attain accurate approximations and rapid convergence.

The paper is broken into five sections: Section 2 introduces the system of interest; Section 3 reviews the weighted residual formulation in time; Section 4 provides an overview of the different basis functions under investigation; Section 5 specifies the unilateral contact model; and Section 6 presents and compares results for a number of basis function combinations.

2. System of interest

A schematic of a simple unilateral contact system showing a one-dimensional bar clamped on the left is depicted in Fig. 1; such systems are known to be well-posed unilateral contact problem [33]. A gap g exists between the tip and a rigid foundation. When the tip displacement is sufficiently large, the bar comes into contact with the rigid foundation and unilateral contact conditions must be satisfied. The existence of periodic solutions of period T are assumed where T is the period of the external forcing $f(x,t)$ acting on the bar. Accordingly, the unknown displacement has to satisfy the following complementary boundary value problem:

1. local equation of motion

$$\rho S \ddot{u}(x,t) + E S u_{,xx}(x,t) = f(x,t), \quad \forall x \in]0, \ell[, \quad \forall t \tag{1}$$

2. conditions of periodicity in time

$$u(x, t+T) = u(x,t) \quad \text{and} \quad \dot{u}(x, t+T) = \dot{u}(x,t), \quad \forall x \in [0, \ell], \quad \forall t \tag{2}$$

3. boundary condition in displacement

$$u(0,t) = 0, \quad \forall t \tag{3}$$

4. unilateral contact conditions

$$g - u(\ell, t) \geq 0 \quad ; \quad \lambda(t) \geq 0 \quad ; \quad \lambda(t) \cdot \big(g - u(\ell, t)\big) = 0, \quad \forall t. \tag{4}$$

Here ρ signifies density, S cross-sectional area, and E elastic modulus. The dot superscript represents a temporal derivative, whereas the subscript x represents a spatial derivative. Structural damping is incorporated later by assuming β-damping of the elastic modulus, as detailed in Section 3.

The periodicity conditions result in a problem which can be formulated on a circle in time. Without loss of generality, the basis functions are taken from an $L^2(\mathbb{S}^1)^N$ Hilbert space [18], where the period of the steady-state solution T has been normalized to 1 [3]. A brief description of the Sobolev spaces used herein can be found in the Appendix.
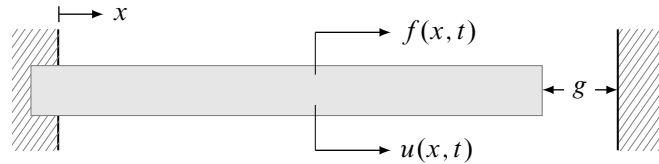

Figure 1. One-dimensional linear bar undergoing unilateral contact conditions

The quantity $\lambda(t)$, that mechanically is a contact force, stems from the enforced non-penetration condition $g - u(\ell, t) \geq 0$ and is necessarily positive (by convention). The complementarity condition

$\lambda(t) \cdot (g - u(\ell, t)) = 0$ states that the contact force $\lambda(t)$ and the distance $g - u(\ell, t)$ separating the rod's end-tip from the rigid foundation may not be zero at the same time. These three conditions are such that the mathematical object pairing the contact force to the displacement is not a function in the usual sense. It is also known that the displacement field may be non-differentiable at given instants within the period of motion and the velocity field may be discontinuous. This motivates the derivation of numerical techniques capable of efficiently handling this nonsmoothness. As a first approach, the unilateral contact inequalities (4) are simplified and replaced by a penalty function; an exponential spring K_p is used to approximate the contact forces. The gap g in Fig. 1 separates the tip of the rod and the exponential spring. The penalty function is of the form

$$f_c(u(\ell, t)) = \max(a_c(e^{\alpha(u(\ell,t)-g_0)} - 1), 0). \tag{5}$$

Specific values for the penalty function are provided with the other model parameters in Section 5.

3. Weighted residual formulations in time

The method of weighted residuals is a classic method of obtaining numerical solutions to boundary value problems by expanding the sought solution as a finite sequence of basis functions in a proper functional space [19], commonly referred to as trial functions. The subsequent residual is rendered orthogonal to a set a linearly independent functions of the same space, referred to as weighting functions, through an inner product. Trial and weighting functions may contain the same basis function but not necessarily: The Galerkin method is a special case where the weighting functions are taken from the same function basis as that of the trial functions; the Petrov-Galerkin method involves the selection of weighting function comprising a basis which is independent of the trial function [14]. The functional space into which the solution is sought is such that the boundary conditions in space and time are satisfied. In this study, the displacement of the investigated rod is numerically sought in various Hilbert spaces of square integrable functions defined on the circle $\mathbb{S}^1$.

To solve Eqs. (1), (2), (3), and (4), the unknown displacement is expanded into a truncated series of N functions separated in space and time:

$$u(x, t) = \sum_{i=1}^{N} \vartheta(x)u_i(t) \tag{6}$$

The standard Finite Element Method is implemented for the spatial variable using two-node linear rod elements [2, 24]. This yields the following vector ordinary differential equation of size N:

$$\mathbf{M}\ddot{\mathbf{u}}(t) + \mathbf{C}\dot{\mathbf{u}}(t) + \mathbf{K}\mathbf{u}(t) = \mathbf{f}_{\text{ext}}(\mathbf{u}(t), t) \tag{7}$$

together with the remaining periodicity conditions in time and the unilateral contact condition. It should be noted that Eq. (7) is an approximate equation of a vibrating structure which may be of one, two or three dimensions. The system is constrained so that condition (3) is now satisfied. Here $\mathbf{M}$ and $\mathbf{K}$ are the standard mass and stiffness matrices for a rod, and β-damping is enforced such that $\mathbf{C} = \beta\mathbf{K}$ to account for structural damping. The displacement vector $\mathbf{u}(t)$ in Eq. (7) stores the temporal unknowns $u_i(t), i = 1, \ldots, N$, where N is the number of spatial degrees-of-freedom. Similarly, $\mathbf{f}_{\text{ext}}(\mathbf{u}(t), t)$ stores the external forcing functions for each degree-of-freedom as well as the contact forces stemming from Eq. (5).

The remainder of the derivation involves a weighted residual formulation in the time dimension. Three forms of the weighted residual method are discussed: the strong integral form, the weak form, and the distributional formulation. For this discussion it is understood that $\mathbf{u}$ and $\mathbf{v}$ are time-dependent vectors, *i.e.* $\mathbf{u}(t)$ and $\mathbf{v}(t)$, but for the sake of clarity the (t) is omitted below.

3.1. Strong integral form

The standard weighted residual formulation of a differential equation is commonly termed the strong form. Taking the inner product of Eq. (7) with a weighting function stored column-wise in $\mathbf{v}$ results in the strong

integral form of the equation: find $\mathbf{u} \in H^2(\mathbb{S}^1)^N$ such that

$$\forall \mathbf{v} \in L^2(\mathbb{S}^1)^N, \quad \int_{\mathbb{S}^1} \left(\mathbf{v}^T \mathbf{M}\ddot{\mathbf{u}} + \mathbf{v}^T \mathbf{C}\dot{\mathbf{u}} + \mathbf{v}^T \mathbf{K}\mathbf{u} - \mathbf{v}^T \mathbf{f}_{\text{ext}}(\mathbf{u}, t) \right) \mathrm{d}t = 0 \tag{8}$$

and the superscript T denotes a transpose. This strong form of the equation is not necessarily the best framework for obtaining a solution [24]; for this example involving a vector ordinary differential equation of order 2, the solution must be at least H^2, limiting the permissible basis of trial functions.

3.2. Weak form

The respective weak form of the weighted residual statement can be obtained by performing one integration by parts over the domain $\mathbb{S}^1$ for all terms containing a double time derivative in Eq. (8). This results in: find $\mathbf{u} \in H^1(\mathbb{S}^1)^N$ such that

$$\forall \mathbf{v} \in H^1(\mathbb{S}^1)^N, \quad \int_{\mathbb{S}^1} \left(-\dot{\mathbf{v}}^T \mathbf{M}\dot{\mathbf{u}} + \mathbf{v}^T \mathbf{C}\dot{\mathbf{u}} + \mathbf{v}^T \mathbf{K}\mathbf{u} - \mathbf{v}^T \mathbf{f}_{\text{ext}}(\mathbf{u}, t) \right) \mathrm{d}t = 0 \tag{9}$$

The integral form of the weak formulation offers the advantage of shifting a portion of the functional smoothness requirement from the trial functions onto the weighting functions. More precisely, both the trial and weighting functions must now be H^1. This allows the trial functions to be chosen from a wider permissible space [24].

3.3. Formulation in a distributional sense

The above procedure of obtaining the solution from the weak formulation by performing integration by parts on the weighted residual statement can be extended one step further. Theoretically, this extension is not necessary since it is known that displacements should be absolutely continuous in time, though it may assist in the numerical derivations and allow very simple basis functions to be considered [38]. A weaker formulation is proposed by integrating again the terms involving time derivatives of the trial functions. This formulation can be understood in the sense of distributions, also known as generalized functions, *ie*: find $\mathbf{u} \in L^2(\mathbb{S}^1)^N$ such that

$$\forall \mathbf{v} \in H^2(\mathbb{S}^1)^N, \quad \int_{\mathbb{S}^1} \left(\ddot{\mathbf{v}}^T \mathbf{M}\mathbf{u} - \dot{\mathbf{v}}^T \mathbf{C}\mathbf{u} + \mathbf{v}^T \mathbf{K}\mathbf{u} - \mathbf{v}^T \mathbf{f}_{\text{ext}}(\mathbf{u}, t) \right) \mathrm{d}t = 0 \tag{10}$$

Here the double time differential on the field variable is transferred to the weighting function and the continuity requirement on the trial function is reduced. As discussed later, the desired displacement functions $\mathbf{u}$ can now be described using a series of constant piecewise functions for instance.

3.4. Time discretization

Let each nodal displacement $u_i(t)$ be approximated by a combination of M linearly independent trial functions $q_k(t)$, $k = 1, \ldots, M$ defined on $t \in [0, 1)$. Similarly, let each $v_i(t)$ be approximated by a combination of linearly independent weighting functions $p_k(t)$, $k = 1, \ldots, M$ also defined on $t \in \mathbb{S}^1$. Collectively, this leads to

$$u_i(t) = \sum_{k=1}^{M} a_{ik} q_k(t), \quad i = 1, \ldots, N \quad \text{and} \quad v_i(t) = \sum_{k=1}^{M} b_{ik} p_k(t), \quad i = 1, \ldots, N \tag{11}$$

or, equivalently in a vector form:

$$\mathbf{u}(t) = \mathbf{\Theta}(t)\mathbf{a} \quad \text{and} \quad \mathbf{v}(t) = \mathbf{\Gamma}(t)\mathbf{b} \tag{12}$$

In Eq. (12), $\mathbf{\Theta}(t)$ and $\mathbf{\Gamma}(t)$ are rectangular matrices of dimension $N \times NM$; $\mathbf{a}$ and $\mathbf{b}$ are vectors of size $NM \times 1$.

Each of the strong, weak, and distributional formulations can now be discretized with proper basis functions. The overall goal of this paper is to discuss the numerical properties of certain wavelet bases to efficiently solve the problem of interest. Depending on the selected formulation, the order of derivation acting on $\mathbf{u}(t)$ and $\mathbf{v}(t)$ (*i.e.* $\mathbf{\Theta}(t)$ and $\mathbf{\Gamma}(t)$ respectively) will affect the admissible basis functions. The corresponding discretized versions are:

- strong integral form:

$$\int_{\mathbb{S}^1} \left((\mathbf{\Gamma}^T \mathbf{M} \ddot{\mathbf{\Theta}} + \mathbf{\Gamma}^T \mathbf{C} \dot{\mathbf{\Theta}} + \mathbf{\Gamma}^T \mathbf{K} \mathbf{\Theta}) \mathbf{a} - \mathbf{\Gamma}^T \mathbf{f}_{\text{ext}}(\mathbf{\Theta} \mathbf{a}, t) \right) dt = 0 \tag{13}$$

- weak form:

$$\int_{\mathbb{S}^1} \left((-\dot{\mathbf{\Gamma}}^T \mathbf{M} \dot{\mathbf{\Theta}} + \mathbf{\Gamma}^T \mathbf{C} \dot{\mathbf{\Theta}} + \mathbf{\Gamma}^T \mathbf{K} \mathbf{\Theta}) \mathbf{a} - \mathbf{\Gamma}^T \mathbf{f}_{\text{ext}}(\mathbf{\Theta} \mathbf{a}, t) \right) dt = 0 \tag{14}$$

- distributional form:

$$\int_{\mathbb{S}^1} \left((\ddot{\mathbf{\Gamma}}^T \mathbf{M} \mathbf{\Theta} - \dot{\mathbf{\Gamma}}^T \mathbf{C} \mathbf{\Theta} + \mathbf{\Gamma}^T \mathbf{K} \mathbf{\Theta}) \mathbf{a} - \mathbf{\Gamma}^T \mathbf{f}_{\text{ext}}(\mathbf{\Theta} \mathbf{a}, t) \right) dt = 0 \tag{15}$$

The resulting nonlinear equations can generically be recast in the following form

$$\mathbf{G} \mathbf{a} - \mathbf{f}(\mathbf{a}) = \mathbf{0} \tag{16}$$

where $\mathbf{G} \mathbf{a}$ and $\mathbf{f}(\mathbf{a})$ respectively stand as the linear internal and the nonlinear external contributions in Eq. (13), (14), and (15).

3.5. Matrix condensation

It is useful to note that after discretization in space and time, the penalty-like contact force is applied solely to the last degree of freedom. This allows the equations of motion to be condensed to a single active degree-of-freedom. Consider the partitioning of Eq. (16) into passive p and active a degrees-of-freedom as follows:

$$\begin{bmatrix} \mathbf{G}_{pp} & \mathbf{G}_{pa} \\ \mathbf{G}_{ap} & \mathbf{G}_{aa} \end{bmatrix} \begin{pmatrix} \mathbf{a}_p \\ \mathbf{a}_a \end{pmatrix} - \begin{pmatrix} \mathbf{f}_p \\ \mathbf{f}_a(\mathbf{a}_a) \end{pmatrix} = \begin{pmatrix} \mathbf{0} \\ \mathbf{0} \end{pmatrix}. \tag{17}$$

In this form, vector $\mathbf{f}_p$ stores the external prescribed periodic forcing acting on the structure while $\mathbf{f}_a(\mathbf{a}_a)$ is the displacement-dependent nonlinear contact force. The first block row of Eq. (17) is linear and gives

$$\mathbf{a}_p = \mathbf{G}_{pp}^{-1} (\mathbf{f}_p - \mathbf{G}_{pa} \mathbf{a}_a) \tag{18}$$

resulting in the condensation equation

$$(\mathbf{G}_{aa} - \mathbf{G}_{ap} \mathbf{G}_{pp}^{-1} \mathbf{G}_{pa}) \mathbf{a}_a + \mathbf{G}_{ap} \mathbf{G}_{pp}^{-1} \mathbf{f}_p - \mathbf{f}_a(\mathbf{a}_a) = \mathbf{0} \tag{19}$$

or

$$\bar{\mathbf{G}} \mathbf{a}_a - \bar{\mathbf{f}}(\mathbf{a}_a) = \mathbf{0} \tag{20}$$

for simplicity. The square matrix and vectors of Eq. (20) are of size M. Eq. (20) is nonlinear and must be solved using an appropriate solver. Condensing the equations of motion to the single active degree of freedom greatly reduces the number of unknowns in the nonlinear solution, reducing computational times and generally increasing the rate of convergence.

4. Trial and weighting function bases

The selection of functional bases to be used in the above approaches is an important factor in approximation accuracy and computational efficiency [2, 24]. *A priori* selection of the optimal bases for unilateral contact problems is not a trivial matter due to potential nonsmoothness of the response. In the current investigation a number of bases are investigated to compare the quality of approximation, including Fourier functions, B-spline wavelets, Daubechies wavelets, and Haar wavelets.

4.1. Harmonic balance and Fourier series

The harmonic balance method (HBM) is a special case of the weighted residual method where the Fourier basis is used for both the trial and weighting functions [27]. This technique is particularly effective when dealing with smooth nonlinear systems; convergence is often reached with very few terms. It has been used to study steady state response of turbine engine blades with friction dampers using a multiterm approximation [39]. This approach was extended to unilateral contact and friction conditions [21] through an Alternating Frequency/Time domain strategy proposed by Cameron *et al.* [9] and Pilipchuk [30]. It is worthy to note that the HBM formulations of Eqs. (13), (14), and (15) are identical.

The Fourier basis for $L^2(\mathbb{S}^1)$ is defined as $\{1\} \cup \{\cos(2m\pi t), \sin(2m\pi t) | m \in \mathbb{N}^*\}$ where m signifies the harmonic number of the function. The first six functions are shown in Fig. 2.
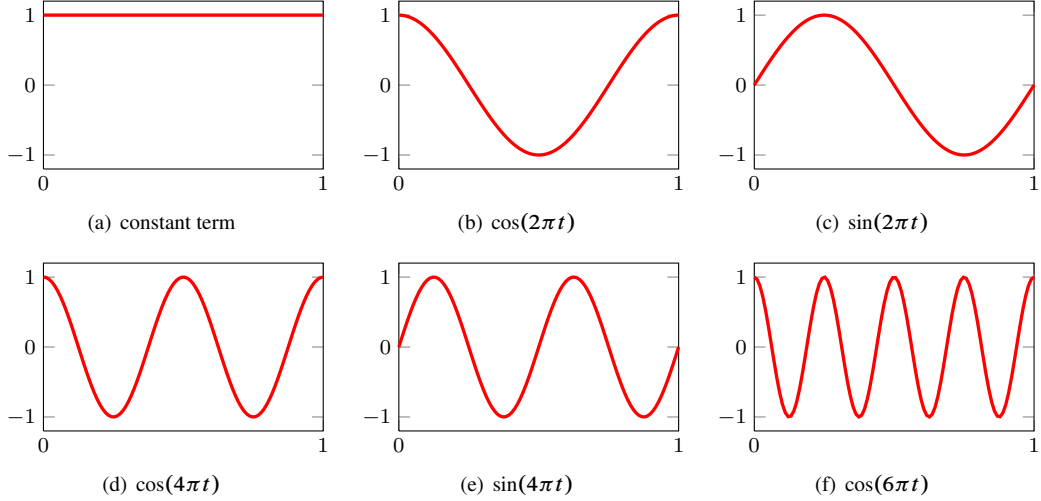

Figure 2. First six functions of the Fourier basis

Fourier basis functions feature an infinite degree of smoothness. While this property can be beneficial in some cases, it is unclear whether Fourier functions are optimal when simulating potentially nonsmooth problems. It is possible that a large number of harmonics would be required to accurately capture the nonsmooth response, or the approximation may exhibit Gibbs phenomenon at localized discontinuities in the sought displacement and velocity fields. Accordingly, other basis functions featuring a lesser degree of functional smoothness are explored.

4.2. Discrete orthogonal wavelets and periodization

Discrete orthogonal wavelet families are composed of highly localized, oscillatory functions which provide a basis of $L^2(\mathbb{R})$ and can be adapted to the periodic domain $L^2(\mathbb{S}^1)$ [25]. These localized characteristics, or compact support, allow sparse representation of piecewise signals including transients and singularities [8]. This makes them useful functions for use in the Galerkin approach when nonsmooth solutions are predicted [37]. There are a large number of wavelet families and definitions thereof; both Mallat [25] and Strang [37] provide excellent introductions to wavelet theory and history. Galerkin methods using appropriate discrete wavelet families as the trial functions have been shown to accurately approximate the solutions to both ordinary and partial differential equations [4, 5, 29, 41, 11, 7].

The discrete wavelet family is built from scaling functions $\phi(t)$ and wavelet functions $\psi(t)$. These functions are analogous to the low-pass and high-pass filters of a filter bank [37]; decomposition using scaling functions will give a "smoothed" approximation of the original signal, while decomposition using wavelet functions provides the details of the signal, or high-frequency content.

The exact decomposition of a continuous time signal $y(t)$ can be written

$$y(t) = \sum_k g_k \phi_{J,k}(t) + \sum_{j=J}^{m} \sum_{\ell} h_{j,\ell} \psi_{j,\ell}(t) \tag{21}$$

and

$$\phi_{J,k}(t) = 2^{J/2}\phi(2^J t - k) \tag{22}$$

$$\psi_{J,k}(t) = 2^{J/2}\psi(2^J t - k) \tag{23}$$

where $J, k \in \mathbb{Z}$; J is the dilation parameter (*i.e.* level), k is the translation parameter, and m is the maximum resolution given by the sampling rate of the function $y(t)$.

The span of the scaling functions at level J is commonly denoted $\mathbf{V}_J$, while the wavelet span is denoted $\mathbf{W}_J$. For orthogonal wavelet families, $\mathbf{W}_J$ is the orthogonal complement to $\mathbf{V}_J$ in $\mathbf{V}_{J+1}$

$$\mathbf{V}_{J+1} = \mathbf{V}_J \oplus \mathbf{W}_J. \tag{24}$$

Provided the wavelet family is orthogonal [37], the space of square-integrable functions on the real line $L^2(\mathbb{R})$ can be decomposed using multiresolution analysis as a nested sequence of closed subspaces [25]

$$\cdots \subset \mathbf{V}_{-2} \subset \mathbf{V}_{-1} \subset \mathbf{V}_0 \subset \mathbf{V}_1 \subset \mathbf{V}_2 \subset \cdots \subset L^2(\mathbb{R}) \tag{25}$$

such that

$$\lim_{J \to \infty} \mathbf{V}_J = L^2(\mathbb{R}). \tag{26}$$

This implies that $\mathbf{V}_J$, the subspace composed of the set of scaling functions at level J, can approximate any function in $L^2(\mathbb{R})$. A reduced orthonormal basis of $L^2(\mathbb{R})$ is constructed by truncating the wavelet terms, resulting in

$$u(t) = \sum_k u_k \phi_{J,k}(t) \tag{27}$$

The accuracy of this approximation increases as the level J is increased. This property of the scaling functions makes them excellent trial and weighting functions in weighted residual methods because they can be adapted to the accuracy level required. The reduced orthonormal basis of scaling functions is used in the current investigation. This approach of increasing the level of scaling functions, rather than including wavelet functions to increase approximation accuracy, is a common approach in the literature [28] and used in the bulk of the applicable references cited in this paper.

Standard wavelet definitions (*i.e.* scaling and wavelet functions) are commonly built on the real line. The functions can be adapted to periodic functions of $L^2(\mathbb{S}^1)$ by utilizing a standard periodization technique [25, 15, 26]. Let $\phi^{(p)}(t)$ be the periodized form of the scaling function $\phi(t)$ defined on $\mathbb{R}$

$$\phi_{J,k}^{(p)}(t) = \sum_{\ell \in \mathbb{Z}} \phi_{J,k}(t - \ell) \qquad 0 \le k \le 2^J - 1. \tag{28}$$

This is equivalent to "wrapping around" the support $\mathbb{R}$ on $\mathbb{S}^1$ through summation. The finite size of the interval results in the condition $J \ge 0$

$$\mathbf{V}_0 \subset \mathbf{V}_1 \subset \mathbf{V}_2 \subset \mathbf{V}_3 \subset \cdots \subset L^2(\mathbb{S}^1) \tag{29}$$

such that

$$\lim_{J \to \infty} \mathbf{V}_J = L^2(\mathbb{S}^1). \tag{30}$$

A number of periodic discrete wavelet families exist [25]. The investigation considers three families to determine how they perform in unilateral, nonsmooth contact problems: B-spline, Daubechies, and Haar.

4.3. Orthogonal cubic B-spline scaling functions

The scaling function ϕ for the orthogonal cubic B-spline wavelet family built on $\mathbb{R}$ is given as [6]

$$\phi(t) = \sum_k c_k B_3(t - k) \tag{31}$$

where cubic B-spline $B_3(t)$ can be written using the following formulas

$$B_3(t) = \begin{cases} t^3/6 & (0 \leq t \leq 1) \\ -t^3/2 + 2t^2 - 2t + 2/3 & (1 \leq t \leq 2) \\ t^3/2 - 4t^2 + 10t - 22/3 & (2 \leq t \leq 3) \\ -t^3/6 + 2t^2 - 8t + 32/3 & (3 \leq t \leq 4) \\ 0 & (\text{otherwise}). \end{cases} \tag{32}$$

The coefficients c_k can be determined using [6]

$$c_k = c_{-k} = \frac{1}{\pi} \int_0^\pi \frac{\cos(k\xi)}{\sqrt{p_3(\cos\xi)}} \, d\xi \qquad (k \geq 0) \tag{33}$$

where k is an integer. The cubic polynomial p_3 is given as

$$p_3(y) = \frac{1}{630}(y^3 + 60y^2 + 297y + 272). \tag{34}$$

Numerical simulations showed that truncating the summation in Eq. (31) at $-50 \leq k \leq 50$ is sufficient; larger k terms add negligibly to the summation. After periodization to $\mathbb{S}^1$ and normalization by $\int_0^1 \phi_{J,k}(t) \, dt = 1$ [10], sample orthogonal cubic B-spline scaling functions for $J = 0, 1, \ldots, 5$ are shown in Fig. 3
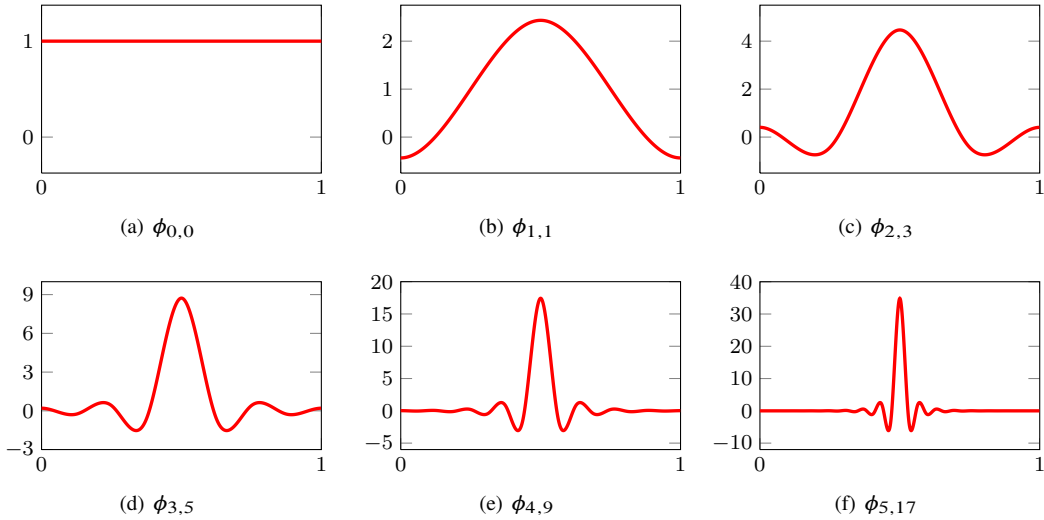

(a) $\phi_{0,0}$ (b) $\phi_{1,1}$ (c) $\phi_{2,3}$

(d) $\phi_{3,5}$ (e) $\phi_{4,9}$ (f) $\phi_{5,17}$

Figure 3. Examples of the first six levels of periodized orthogonal cubic B-spline scaling functions

4.4. Daubechies Wavelets

The Daubechies wavelet family is defined by a set of L filter coefficients $\{p_\ell : \ell = 0, 1, \ldots, L - 1\}$, where L is an even integer. The scaling function is defined by the fundamental two-scale equation [10]

$$\phi(t) = \sum_{\ell=0}^{L-1} p_\ell \, \phi(2t - \ell) \tag{35}$$

8

which has fundamental support over the finite intervals $[0, L-1]$. This equation can be used to determine the value of the scaling function at dyadic points $t = n/2^J$, $n = 0, 1, \ldots$ using the algorithm provided by Chen *et al.* [10].

The wavelet filter coefficients p_ℓ were derived by Daubechies to produce scaling and wavelet functions with specific properties [10, 12], some of which include:

- the area under the scaling function is unity

$$\int_{-\infty}^{\infty} \phi(t)\,\mathrm{d}t = 1 \tag{36}$$

- the coefficients sum to two

$$\sum_{\ell=0}^{L-1} p_\ell = 2 \tag{37}$$

- the scaling function and its translates are orthogonal

$$\int_{-\infty}^{\infty} \phi(t)\phi(t-k)\,\mathrm{d}t = \delta_{0,k} \qquad k \in \mathbf{Z} \tag{38}$$

The corresponding scaling functions are highly nonsmooth and fractal in nature: as one increases the resolution of the functions, the shape does not converge but rather continues to increase in complexity. This makes accurately estimating the inner products of such scaling functions with each other prone to error when numerical integration is used [32].
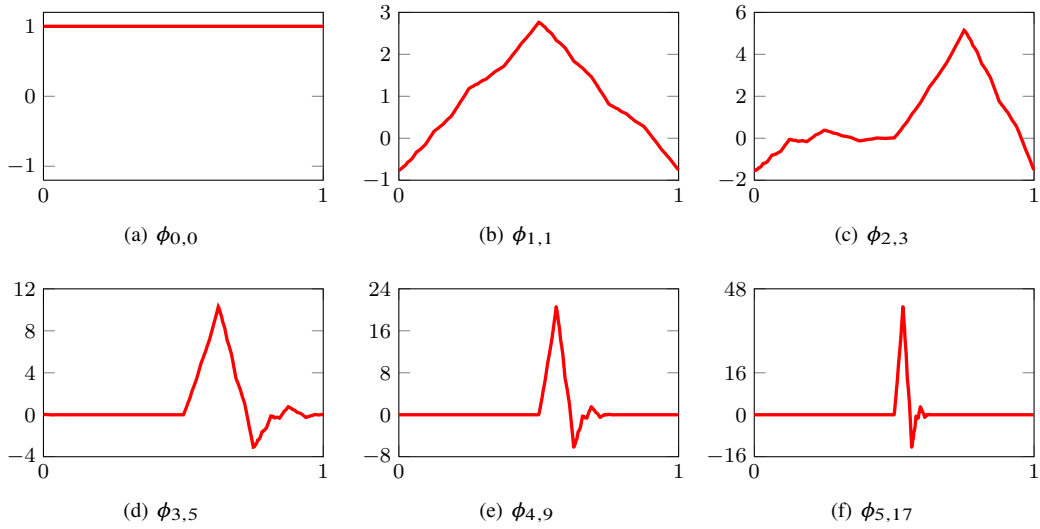

Figure 4. Examples of the first six levels of periodized 6 coefficient Daubechies scaling functions (DB6)

When Daubechies scaling functions are used in a Galerkin approach, it is necessary to derive the inner products of the scaling function with itself or derivatives of itself. The exact solution to these inner products can be found by using the recursive nature of the fundamental equation on $L^2(\mathbb{R})$ [4, 10]; the solution to these inner products are commonly referred to as connection coefficients. When Daubechies scaling functions are periodized on $\mathbb{S}^1$, the wrapping procedure results in functions which are no longer scale-invariant at low J values (scale-invariance requires wavelets at any scale to be a pure dilation of the mother-wavelet). Fig. 4 provides examples of the periodized scaling functions for $L = 6$. Interestingly, the lack of scale-invariance for small J values does not invalidate the connection coefficient algorithms derived for unbounded domains; the connection coefficients can simply be wrapped around the periodic domain as necessary [32].

4.5. Haar scaling functions

The simplest Daubechies wavelet family requires only two filter coefficients ($p_0 = p_1 = 1$) and is commonly known as the Haar wavelet family [17]. The Haar scaling functions are rectangular tophat-type functions; the father scaling function is defined on $t \in \mathbb{R}$ as

$$\phi(t) = \begin{cases} 1 & (0 \le t < 1) \\ 0 & (\text{otherwise}). \end{cases} \tag{39}$$

Since the compact support of the father scaling function is $\mathbb{S}^1$, the periodized function is equivalent. Example Haar scaling functions for $J = 0, 1, \ldots, 5$, normalized by Eq (36), are shown in Fig. 5.
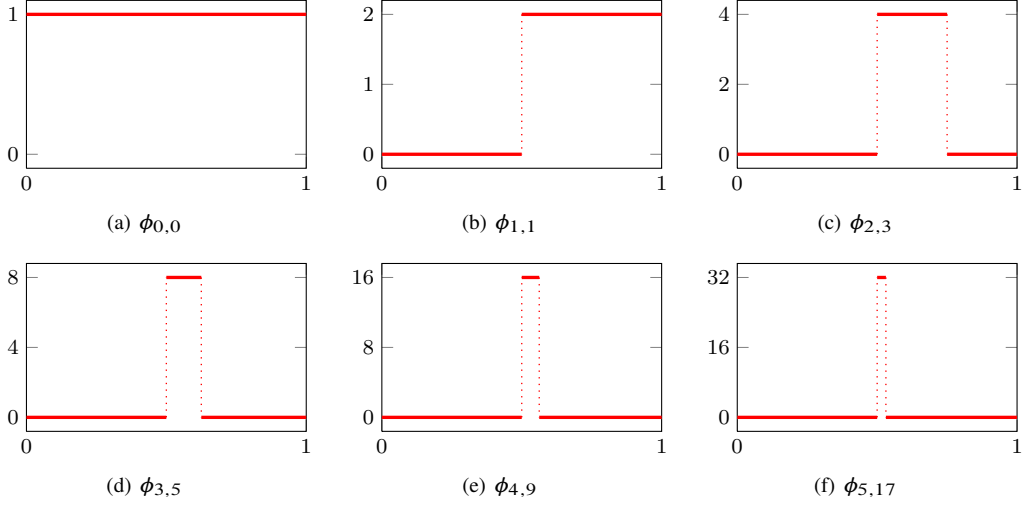
Figure 5. Examples of the first six levels of periodized Haar scaling functions

5. Model development

The mixed finite-element/wavelet-Galerkin model of the axial bar undergoing unilateral contact introduced in Section 2 has the following properties: elastic modulus $E = 70$ GPa; cross-sectional area $S = 25$ cm^2; density $\rho = 2700$ kg/m^3; total length $L = 1$ m; external force amplitude $F = 250kN$; and damping factor β. A total of 25 finite elements are used. The fundamental frequency of this rod is approximately 1273 Hz.

The values of a_c and α in Eq. (5) were selected to simulate a reasonably rigid penalty function while maintaining good conditioning of the system of nonlinear equations. Table 1 lists the two forcing frequency cases considered: 150 Hz and 1275 Hz. The maximum tip displacements without contact for this system are approximately 1.4 mm at 150 Hz and 29 mm at 1275 Hz.

	Case 1	Case 2
forcing frequency	150 Hz	1275 Hz
penalty constant, a_c	1×10^8	1×10^8
penalty exponent, α	50	20
damping factor, β	1×10^{-4}	5×10^{-6}
initial gap, g_0	1.0 mm	14.5 mm

Table 1. Test cases

To act as a comparison solution, the unilateral contact finite-element equations detailed above are solved using a variable-order numerical differentiation formula (NDF) time-stepping algorithm [35]. As the time-stepping solution does not solve for the periodic response directly, the solution is deemed to have

converged to its periodic state when the rms of the relative error between the tip displacements for the i and $i-1$ periods is below 10^{-7}. This is possible due to the structural damping terms listed in Table 1 causing any transient response to decay relatively quickly.

Table 2 lists the combination of trial and weighting functions employed in the current investigation; where wavelet families are listed (B-spline, Haar, Daubechies), it is implied the scaling functions are used according to Eq. (27). The integrals involved in Eq. (16) are computed as discrete inner products using

Trial function	Weighting function
Fourier	Fourier
B-spline	B-spline
Daubechies 6	Daubechies 6
Haar	Fourier
Daubechies 6	Fourier
Haar	B-spline

Table 2. List of trial and weighting function combinations

256 points for all but the Galerkin formulations using Daubechies functions. For the Daubechies Galerkin cases, the inner products are derived using the connection coefficients as mentioned in Section 4.4.

6. Results

The six combinations of trial and weighting functions listed in Table 2 are employed to solve the condensed, nonlinear weighted residual formulation given in Eq. (20) for forcing frequencies of 150 Hz and 1275 Hz.

6.1. Tip displacement

Samples of the approximate tip displacement responses at 150 Hz at 1275 Hz using 64 (*i.e* $J = 6$) basis functions are provided in Fig. 6 and Fig. 7, respectively.
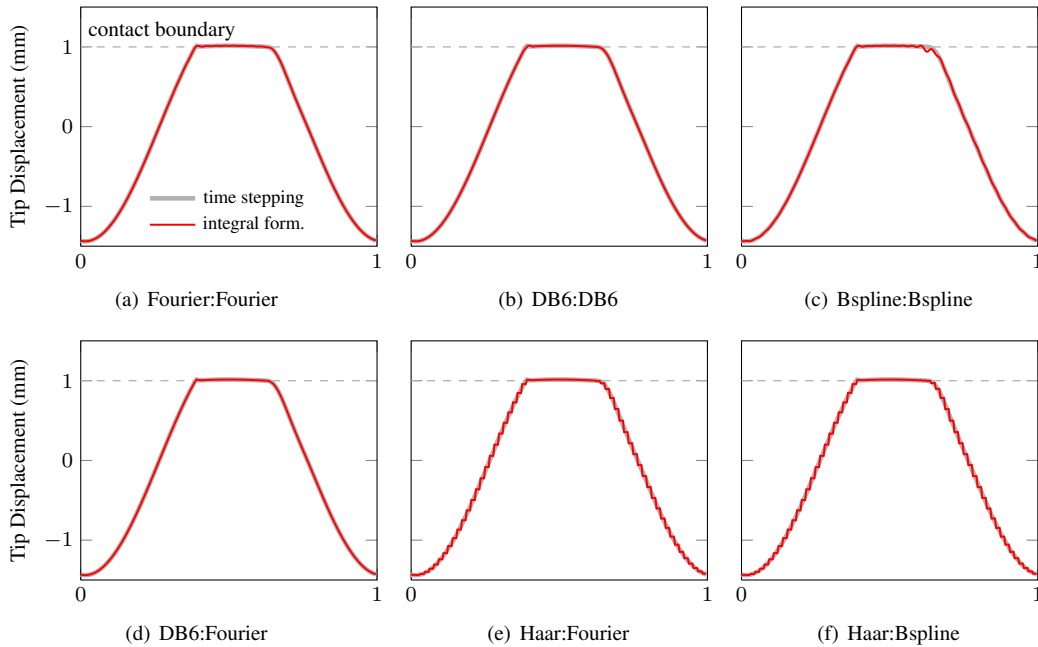

Figure 6. Tip displacement versus normalized time t for Case 1

For this number of basis functions HBM (Fourier:Fourier) approximates the tip displacements well at both 150 Hz and 1275 Hz compared to the time-stepping solution. However, close examination of the
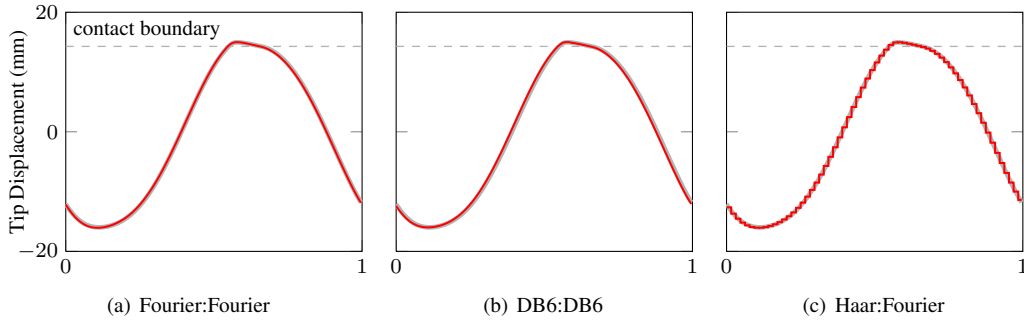
11

Figure 7. Tip displacement versus normalized time t for Case 2

contact plateau for the 150 Hz case shows oscillations due to Gibbs phenomenon and rounding off of the sharp gradient changes. This will be further discussed in Section 6.3.

Alternatively, the Haar:Fourier combination appears to approximate the tip displacement outside the contact zone less well due to the blocky nature of the Haar scaling functions. However, the contact plateau is well represented by the constant Haar scaling functions. The Haar basis appears to be less suited for the response at 1275 Hz as the contact plateau is smaller and not as flat; the tip penetration through the contact boundary is a result of the inexact modeling of hard contact using the exponential spring penalty function. At 1275 Hz, unprovided remaining combinations DB6:Fourier, B-spline:B-spline and Haar:B-spline show tip displacement similar to figure 7.

6.2. Tip velocity

Consideration is also given to the accuracy with which the trial functions considered can determine velocities. For all displacement approximations where the trial basis functions can be differentiated pointwise to approximate velocities using Eq. (11), the following equality is used:

$$\dot{u}_i(t) = \sum_{k=1}^{M} a_{ik} \dot{q}_k(t). \tag{40}$$

The only cases where Eq. (40) is not valid are those involving Haar trial functions; Haar scaling functions are piecewise constant functions thus they cannot be directly differentiated in the usual sense (*i.e.* pointwise) to determine velocities. Velocities for these cases can be approximated by assuming the derivative of a Haar scaling function is the combination of a positive delta function at t_1 and a negative delta function at t_2, where t_1 corresponds to the positive jump discontinuity in the Haar scaling function and t_2 corresponds to the negative jump. Using a set of these functions as $\dot{q}_k(t)$ in Eq. (40) provides a reasonable approximation to the corresponding velocity field for cases involving Haar functions.

The approximate tip velocity response at 150 Hz is plotted in Fig. 8 for all cases using 64 basis functions. It is visible from these approximations that there is a sharp jump in velocity due to the contact condition. As expected, this results in ringing due to Gibbs phenomenon when the Fourier trial functions are used. Interestingly, the ringing is more pronounced in the Galerkin B-spline case. The DB6 trial functions appear to do the best job of approximating the tip response. This is attributed to the compact support of the scaling functions allowing accurate representation of rapid changes in gradient. For cases involving Haar trial functions the velocity function envelope is reasonably approximated by the delta function representation discussed above.

6.3. Tip contact force

The tip contact force is calculated using the penalty function provided in Eq. (5) in conjunction with the predicted tip displacement and presented in Fig. 9; the contact force has been normalized by the magnitude of the external force input. Notice the time duration of the contact forces coincide with the tip displacement plateaus of Fig. 6 as this is the only period during which the tip is in contact with the rigid foundation.
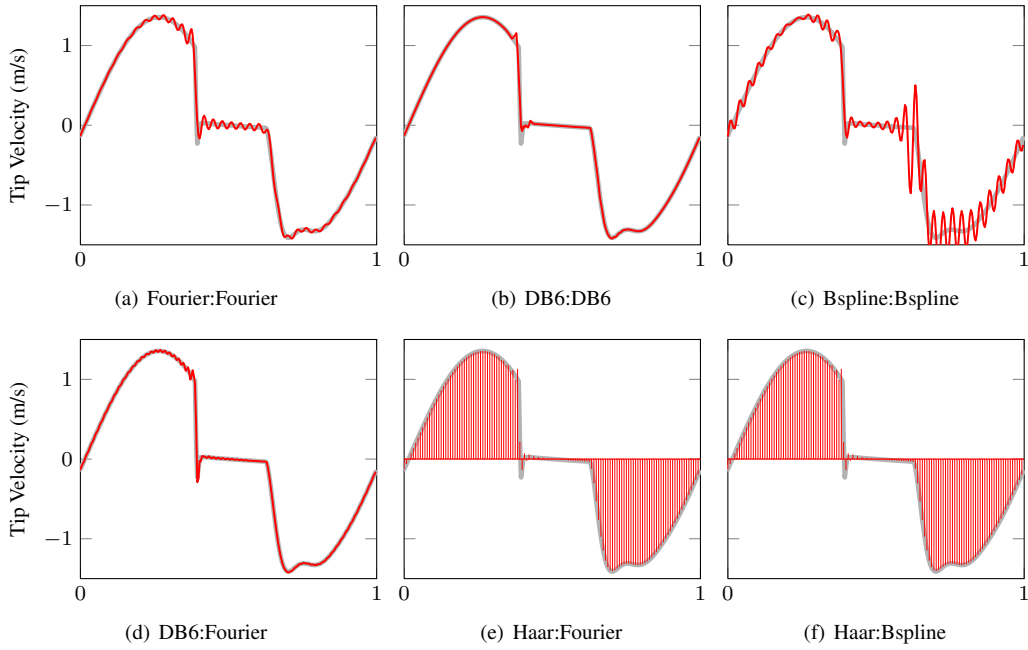
12

Figure 8. Tip velocity versus normalized time t for Case 1

The effect of Gibbs phenomenon can be seen in the HBM and Galerkin B-spline cases. The cases where Haar trial functions are used approximate the contact force relatively well. It is hypothesized that when a rigid contact law is enforced the Haar scaling functions will perform even better relative to the other functions; this will be investigated in future work. Again, the DB6 trial functions appear to most accurately approximate the contact forces compared to the other cases.

6.4. Energy norm convergence

Convergence of the normalized energy norms for each basis combination at 150 Hz and 1275 Hz are given in Fig. 10(a) and 10(b), respectively. For these results the distributional form of the governing equations are used in all cases. Results using the strong and weak forms of the governing equation are discussed further in Section 6.6.

The system energy is calculated as

$$E = \frac{1}{2}\dot{\mathbf{u}}^T\mathbf{M}\dot{\mathbf{u}} + \frac{1}{2}\mathbf{u}^T\mathbf{K}\mathbf{u}. \tag{41}$$

The scalar energy norm is calculated as the rms value of the system energy E over a single period; this is then normalized by the energy norm from the time-stepping solution. The velocity terms $\dot{\mathbf{u}}$ are calculated as detailed in Section 6.2.

As shown in Fig. 10, all combinations of trial and weighting functions converge to values similar to the time-stepping solution (*i.e.* energy norms are approximately unity using 128 basis functions). At 150 Hz, the HBM and Galerkin B-spline approaches show energy norms close to unity even using relatively few basis functions. The Petrov-Galerkin combinations utilizing Haar trial functions over-predict the system energy when few trial functions are used. This is evident in Fig. 6(e) where the blocky nature gives a coarse representation of the periodic response, thus affecting the resulting energy norm. An interesting comparison is between the DB6:DB6 and the DB6:Fourier curves. When Fourier functions are used as the weighting functions, the energy norm is better approximated. This implies projecting the residuals onto the Fourier basis, which has been shown to represent the solution relatively well, increases the accuracy of the prediction.

At 1275 Hz, the six combinations converge to a common energy norm more slowly than at the lower forcing frequency. In this case the HBM and Galerkin B-spline approaches again converge quickly to
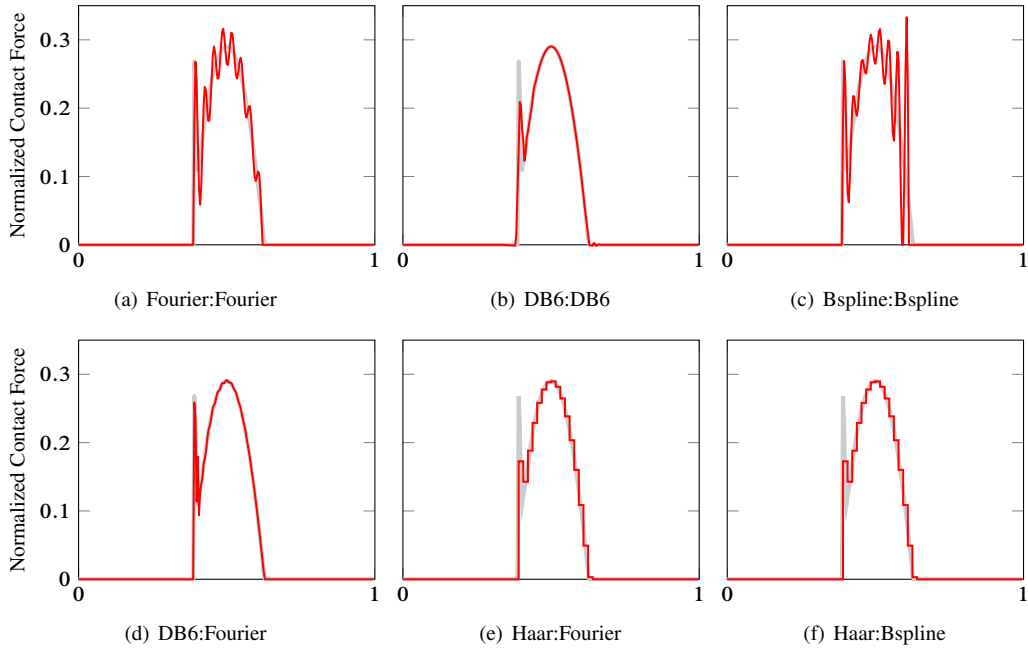
Figure 9. Normalized contact force versus normalized time t for Case 1

the time-stepping solution. The cases with Haar trial functions show larger difference with respect to the normalizing solution than that for the 150 Hz case. This is attributed to the displacement response at this frequency (see Fig. 7(c)); there is no distinct contact plateau thus the Haar trial functions do not approximate the solution as closely as the 150 Hz case. Finally, it is less obvious now that DB6:Fourier combination out performs the DB6:DB6 method at fewer basis functions.

6.5. Tip displacement relative error

It is also desirable to quantify the approximation error for the tip displacements predicted using the weighted residual combinations where the time-stepping solution is again used as a comparison solution. It provides a good relative measure to compare the accuracy of trial:weighting function combinations. The rms error over one period is plotted for the six basis function combinations in Fig. 11(a) for 150 Hz and Fig. 11(b) for 1275 Hz.

As shown in Fig. 11(a), the HBM and Galerkin B-spline approaches have the lowest error when only 8 basis functions are used. This supports the convergence behaviour noted above for these combinations. As the number of basis functions is increased, the Galerkin B-spline case does not perform as well as the HBM method. This is attributed to a localized error which was found to develop at the end of the contact plateau (see Fig. 6(c)). The Galerkin DB6 case performs poorly using 16 trial functions, but rapidly improves to relative error values comparable to the HBM method. The ability of the nonsmooth DB6 scaling functions to accurately predict both the smooth portions of the response as well as the sharp gradient variation is attributed to both the compact support and vanishing moment properties of the the Daubechies functions. The relative error using Haar trial functions is highest out of the combinations investigated. This is expected due to the blocky nature of the Haar scaling functions; however the mid-points of the Haar functions match very well to the trend of the time-stepping solution. This suggests that if only a low resolution approximation of the response is required, the Haar scaling functions still perform well.

The relative error at 1275 Hz shows similar trends to those discussed at 150 Hz. One important difference is the Galerkin B-spline error as the number of basis functions increases: as the unknowns are increased from 32 to 128, the relative error stays reasonably constant. This suggests that this combination of basis functions has reached its limit of prediction accuracy.
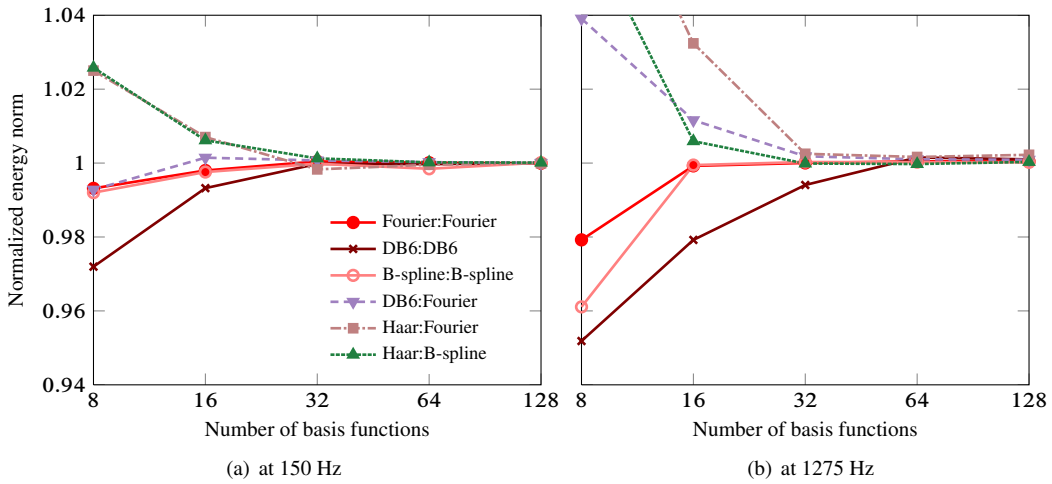
14

(a) at 150 Hz   (b) at 1275 Hz

Figure 10. System energy norm convergence using six trial:weighting function combinations

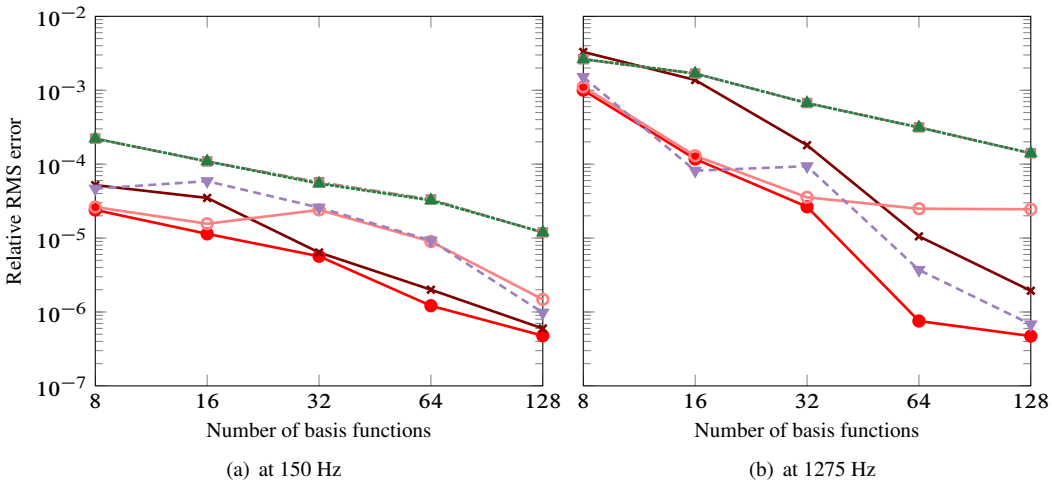(a) at 150 Hz   (b) at 1275 Hz

Figure 11. rms of the relative approximation error between trial:weighting function combinations and the time-stepping solution

6.6. Principal Angles Between Subspaces

The Galerkin and Petrov-Galerkin approaches require the projection of the trial function basis (and/or its derivative) onto the weighting function basis (and/or its derivative); it is within this projected space that the approximate solution is determined. Increasing the dimensionality of either the trial or weighting functional bases will only improve the prediction accuracy provided they expand the approximate solution space to encapsulate more of the actual solution space.

Principal angles provide a measure of the commonality or "overlap" of the two functional spaces. Shonkwiler [36] shows that there are an equal number of principal angles as trial (or weighting) functions. If two sets of basis functions span the same space, all the principal angles will equal zero; if the two sets of basis functions are orthogonal to each other, all the principal angles will equal 90° and the approximate solution space will be null. The more principal angles with values close to 0 implies the projection of the trial functions onto the weighting functions span a larger approximate solution space and thus can potentially provide more accurate predictions.

The principal angles for the six Galerkin and Petrov-Galerkin combinations with 64 degrees of freedom are provided in Fig. 12 for the three projections required in the weaker form (distributional approach)
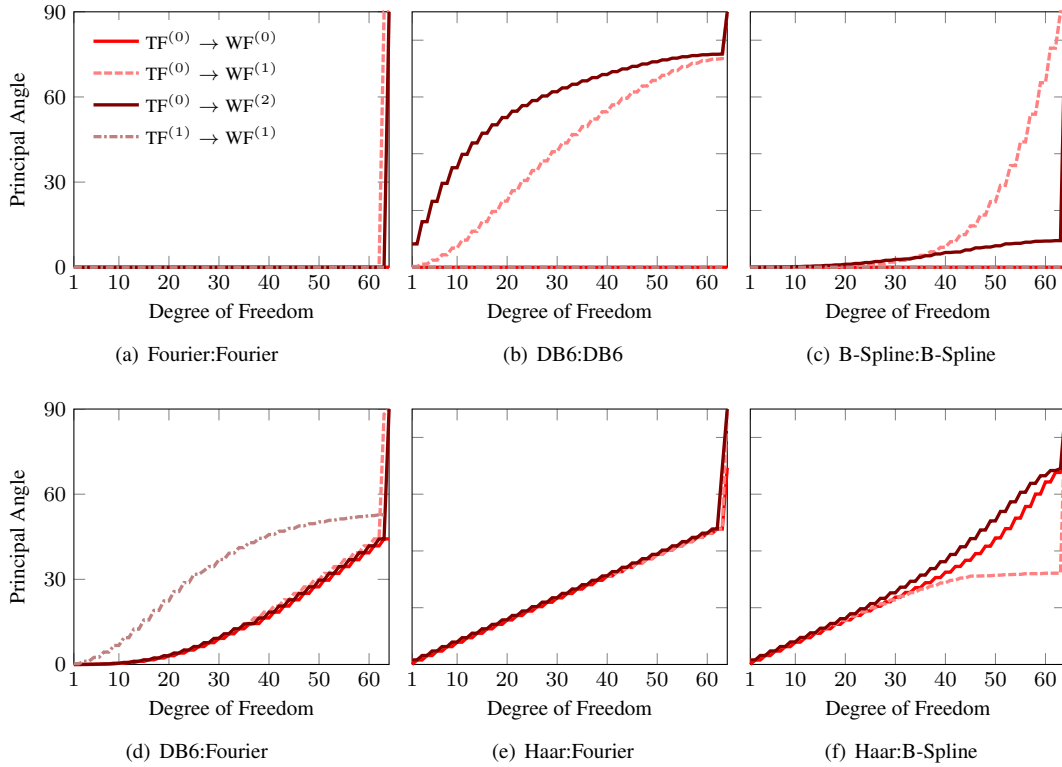
15

Figure 12. Principal angles for Galerkin and Petrov-Galerkin subspaces with 64 degrees of freedom. $TF^{(n)}$ signifies the derivative order of the trial function; $WF^{(n)}$ signifies the derivative order of the weighting function

outlined in Section 3.3: $TF^{(0)} \rightarrow WF^{(0)}$; $TF^{(0)} \rightarrow WF^{(1)}$; $TF^{(0)} \rightarrow WF^{(2)}$. For example, $TF^{(0)} \rightarrow WF^{(1)}$ signifies the trial function basis being projected onto the first derivative of the weighting function basis. Also included are the principal angles for $TF^{(1)} \rightarrow WF^{(1)}$ which is required if the weak form is used.

As expected the Fourier:Fourier combination has principal angles equal to zero for all but a couple of dimensions. Consider $TF^{(0)} \rightarrow WF^{(2)}$ for example: the trial function basis contains the 0th Fourier term (*i.e.* the constant offset vector), whereas in the second derivative of the weighting functions this vector is null. Thus when $TF^{(0)}$ is projected onto $WF^{(2)}$ the information contained in the 0th Fourier term is lost, hence the single 90° principal angle value. All other basis vectors are shared by both spaces so the remaining 63 principal angles are nil as illustrated in Fig. 12(a).

This property is not shared for all Galerkin bases. In Fig. 12(c) the principal angles for the B-Spline Galerkin method are shown and have a greater range than the Fourier:Fourier case. This implies the projected solution space is somewhat smaller for the B-Spline Galerkin approach. This aides in the explaining why the relative errors shown in Fig. 11(a) and 11(b) are larger for B-Spline:B-Spline vs. Fourier:Fourier.

Note that for all the Galerkin combinations $TF^{(0)} \rightarrow WF^{(0)}$ and $TF^{(1)} \rightarrow WF^{(1)}$ the principal angles are all zero. This is because for these cases the trial and weighting function bases are the same. This implies the well-known fact that the weak formulation may provide better prediction accuracy than the distributional formulation, where $TF^{(0)} \rightarrow WF^{(2)}$ is required. Numerical simulation verifies this hypothesis, but the improvement in accuracy is orders of magnitude less than the relative error thus results for the weak form are not included.

For the Petrov-Galerkin cases shown in Fig. 12(e) to 12(f), all the required projections result in a reduction of the solution space. The combinations involving Haar functions as the trial basis appear to have the largest mean principal angles, which attests to the Haar:Fourier and Haar:B-Spline combinations performing poorly according to Fig. 11(a) and 11(b).

16

6.7. Frequency response curve

Another feature of interest is the ability to construct the frequency response function for the unilateral contact condition. The penalty function simulating contact is effectively a stiffening condition, thus the resonant peaks for the system are expected to increase in frequency relative to the no-contact response. To capture this nonlinear response an arc-length continuation method [16] is utilized. The frequency response function over the system's fundamental frequency is shown in Fig. 13 using both the Fourier:Fourier and Haar:Fourier combinations with 64 basis functions.
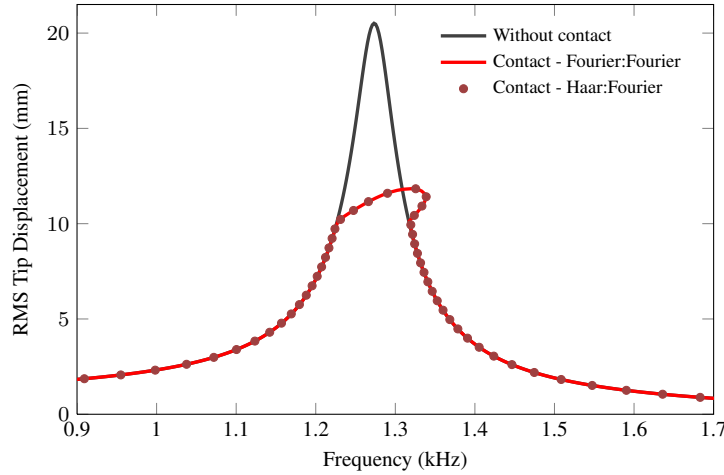
Figure 13. Frequency response function over the 2nd fundamental frequency of the unilateral contact system

As shown, the stiffening behaviour of the unilateral contact condition is captured by both trial:weighting function combinations; other combinations showed similar approximations. These results are promising as it implies the arc-length continuation method can be accurately applied to both Galerkin and Petrov-Galerkin approaches using the distributional formulation for a number of different bases.

7. Conclusions

The method of weighted residuals for capturing the periodic responses of unilateral contact problems has been investigated for a number of trial:weighting function combinations. The contact condition is simulated using an exponential penalty function approach. To extend the allowable trial function bases, a weak and a distributional formulations are presented which transfer trial function continuity requirements to the weighting functions. This allowed piecewise constant Haar scaling functions to be used as a trial basis in the current investigation. Results show that a number of trial:weighting function combinations produce accurate solutions which rapidly converge as the size of the discrete spaces is increased. As expected, Fourier functions perform well as a trial basis, though nonsmooth functions such as Haar and Daubechies scaling functions are also attractive since they provide comparable prediction accuracy and even out perform the Fourier functions in some measures. It is also shown that all the basis combinations considered can be used in an arc-length continuation framework to capture the nonlinear frequency response of the unilateral contact problem.

Research is continuing on this subject. The goal is to improve on the penalty approach by implementing an exact unilateral contact Lagrange multiplier method. This will result in perfectly flat contact plateaus within the periodic response. The major hypothesis is that nonsmooth trial functions will be able to approximate these flat sections better than Fourier functions, and then could provide better contact force estimation and improved convergence for nonlinear solution algorithms.

Furthermore, the results from this investigation show that the prediction accuracy using wavelet scaling functions increases at a similar rate to Fourier function when the global scale is increased. However, this global scale increase may not be optimal. In most cases the coarse wavelet functions can reasonably predict general trends in the response, it is only locations of sharp gradient changes where fine scale functions

are required (*i.e.* very short compact support); this local increase in resolution is not possible with Fourier trial functions [23]. Future work will focus on resolving only these high gradient areas using wavelets and leaving coarse scaling functions to describe the smooth sections. Increased accuracy shall be met while minimizing the number of basis functions required.

Industrial applications involving more complicated contact interface geometries are also targeted.

8. Acknowledgements

A. Sobolev spaces

In the paper, $\mathbb{S}^1$ denotes the circle compact support that can be identified to the interval $(0, 1)$ on the real line. Due to the periodicity conditions in time that should be satisfied by the solution, integral forms are readily derived on this set.

Below is a list of the Sobolev spaces defined on $\mathbb{S}^1$ with brief descriptions on how they relate to the current investigation:

- $L^2(\mathbb{S}^1)$ is the space of square integrable functions on the circle.

- $H^1(\mathbb{S}^1)$ is the space of square integrable functions on the circle in which the first derivative (in a distributional sense) is also square integrable.

- $H^2(\mathbb{S}^1)$ is the space of square integrable functions on the circle in which the first and second derivatives (in a distributional sense) are also square integrable.

- $L^2(\mathbb{S}^1)^N$ is the space containing N square integrable functions on the circle, where N is the number of spatial degrees of freedom in the current investigation—this is analogous for $H^1(\mathbb{S}^1)^N$ and $H^2(\mathbb{S}^1)^N$.

References

[1] Vincent Acary and Bernard Brogliato. *Numerical methods for nonsmooth dynamical systems: Applications in mechanics and electronics*. Volume 35. Lecture Notes in Applied and Computational Mechanics. Springer, 2008. ISBN: 3540753915.
DOI: 10.1007/978-3-540-75392-6.
OAI: hal.inria.fr:inria-00423530.

[2] Klaus-Jürgen Bathe. *Finite element procedures in engineering analysis*. Englewood Cliff: Prentice-Hall, 1996. ISBN: 0133014584.

[3] Sterling Berberian. *Introduction to Hilbert space*. Providence: AMS Chelsea Publishing, 1999. ISBN: 0821819127.

[4] Gregory Beylkin. "On the representation of operators in bases of compactly supported wavelets". *SIAM Journal on Numerical Analysis* 29.6 (1992), 1716–1740.
DOI: 10.1137/0729097.

[5] Gregory Beylkin and James Keiser. "On the adaptive numerical solution of nonlinear partial differential equations in wavelet bases". *Journal of Computational Physics* 132.2 (1997), 233–259.
DOI: 10.1006/jcph.1996.5562.

[6] Christian Blatter. *Wavelets: a primer*. A K Peters/CRC Press, 1998. ISBN: 1568811950.

[7] Rodrigo Burgos, Raul e Silva, and Marco Santos. "Direct solution of differential equations using the wavelet-Galerkin method". *Mecanica Computacional* XXIX (2010). Edited by Eduardo Dvorkin, Marcela Goldschmit, and Mario Storti, 4573–4584.

[8] Sydney Burrus, Ramesh Gopinath, and Haitao Guo. *Introduction to wavelets and wavelet transforms: a primer*. Upper Saddle River: Prentice Hall, 1998. ISBN: 0134896009.

[9] Timothy Cameron and Jerry Griffin. "An alternating frequency/time domain method for calculating the steady-state response of nonlinear dynamic systems". *Journal of Applied Mechanics, Transactions ASME* 56.1 (1989), 149–154.
DOI: 10.1115/1.3176036.

[10] Ming-Quayer Chen, Chyi Hwang, and Yen-Ping Shih. "The computation of wavelet-Galerkin approximation on a bounded interval". *International Journal for Numerical Methods in Engineering* 39.17 (1996), 2921–2944.
DOI: 10.1002/(SICI)1097-0207(19960915)39:17<2921::AID-NME983>3.0.CO;2-D.

[11] Mark Christon and David Roach. "The numerical performance of wavelets for PDEs: the multi-scale finite element". *Computational Mechanics* 25.2-3 (2000), 230–244.
DOI: 10.1007/s004660050472.

[12] Ingrid Daubechies. *Ten lectures on wavelets*. CBMS-NSF Regional Conference Series in Applied Mathematics. Philadelphia: Society for Industrial and Applied Mathematics, 1992. ISBN: 0898712742.
DOI: 10.1137/1.9781611970104.

[13] David Demailly, Fabrice Thouverez, and Louis Jézéquel. "Unbalance Responses of Rotor/Stator Systems with Nonlinear Bearings by the Time Finite Element Method". *International Journal of Rotating Machinery* 10.3 (2004), 155–162.
DOI: 10.1155/S1023621X04000168.

[14] Dale Durran. *Numerical Methods for Fluid Dynamics. With Applications to Geophysics*. 2nd edition. Volume 32. Texts in Applied Mathematics. New York: Springer, 2010. ISBN: 1441964118.

[15] Gordon Erlebacher, Yousuff Hussanini, and Leland Jameson. *Wavelets: Theory and applications*. New York: Oxford University Press, 1996. ISBN: 0195094239.

[16] Gotz von Groll and David Ewins. "The harmonic balance method with arc-length continuation in rotor/stator contact problems". *International Journal for Numerical Methods in Engineering* 241.2 (2001), 223–233.
DOI: 10.1006/jsvi.2000.3298.

[17] Alfréd Haar. "Zur Theorie der orthogonalen Funktionensysteme Erste Mitteilung". *Mathematishe Annalen* 69.3 (1910), 331–371.

[18] Matthias Holschneider. "Wavelet analysis on the circle". *Journal of Mathematical Physics* 31.1 (1990), 39–44.
DOI: 10.1063/1.528825.

[19] Leon Lapidus and John Seinfeld. *Numerical solution of ordinary differential equations*. New York: Academic Press, 1971. ISBN: 0124366503.

[20] Denis Laxalde and Mathias Legrand. "Nonlinear modal analysis of mechanical systems with frictionless contact interfaces". *Computational Mechanics* 47.4 (2011), 469–478.
DOI: 10.1007/s00466-010-0556-3.
OAI: hal.archives-ouvertes.fr:hal-00492775.

[21] Mathias Legrand, Sébastien Roques, Christophe Pierre, Patrice Cartraud, and Bernard Peseux. "*n*-dimensional Harmonic Balance Method extended to non-explicit nonlinearities". *Revue Européenne de Mécanique Numérique* 15.1-2-3 (2006), 269–280.
DOI: 10.3166/remn.15.269-280.
OAI: hal.archives-ouvertes.fr:hal-00354486.

[22] Remco Leine and Henk Nijmeijer. *Dynamics and bifurcations of non-smooth mechanical systems*. 2nd edition. Volume 18. Lecture Notes in Applied and Computational Mechanics. Springer, 2006. ISBN: 3540219870.

[23] Xin Li, Bo Hu, Xie-Ting Ling, and Xuan Zeng. "A wavelet balance approach for steady-state analysis of nonlinear circuits". *The 2001 IEEE International Symposium on Circuits and Systems*. Volume 3. 2. 2001, 73–76.
DOI: 10.1109/ISCAS.2001.921249.

[24] Gui Rong Liu and Siu Sin Quek. *Finite element method: a practical course*. Oxford: Butterworth-Heinemann, 2003. ISBN: 0750658665.

[25] Stéphane Mallat. *A wavelet tour of signal processing. The Sparse Way*. 3rd edition. Amsterdam: Elsevier/Academic Press, 2009. ISBN: 0123743702.

[26] Yves Meyer. *Ondelettes. Ondelettes et opérateurs*. Volume 1. Paris: Hermann, 1990. ISBN: 2705661255.

[27] Ronald Mickens. "Comments on the method of harmonic balance". *Journal of Sound and Vibration* 94.3 (1984), 456–460.
DOI: 10.1016/S0022-460X(84)80025-5.

[28] Ole Møller Nielsen. "Wavelets in Scientific Computing". PhD thesis. Technical University of Denmark, 1998.
OAI: `tel.archives-ouvertes.fr:tel-00803835`.

[29] Stéphane Pernot and Claude-Henri Lamarque. "A wavelet-Galerkin procedure to investigate time-periodic systems: transient vibration and stability analysis". *Journal of Sound and Vibration* 245.5 (2001), 845–875.
DOI: `10.1006/jsvi.2001.3610`.

[30] Valery Pilipchuk. "Application of special nonsmooth temporal transformations to linear and nonlinear systems under discontinuous and impulsive excitation". *Nonlinear Dynamics* 18.3 (1999), 203–234.
DOI: `10.1023/A:1008331427364`.

[31] George Reddien. "Projection methods for two-point boundary value problems". *SIAM Review* 22.2 (1980), 156–171.

[32] Juan Mario Restrepo and Gary Leaf. "Inner product computations using periodized Daubechies wavelets". *International Journal for Numerical Methods in Engineering* 40.19 (1997), 3557–3578.
DOI: `10.1002/(SICI)1097-0207(19971015)40:19<3557::AID-NME227>3.0.CO;2-A`.

[33] Michelle Schatzman and Michel Bercovier. "Numerical Approximation of a Wave Equation with Unilateral Constraints". *Mathematics of Computation* 53.187 (1989), 55–79.

[34] Thorsten Schindler and Vincent Acary. "Timestepping schemes for nonsmooth dynamics based on discontinuous Galerkin methods: Definition and outlook". *Mathematics and Computers in Simulation* (2012).
DOI: `10.1016/j.matcom.2012.04.012`.
OAI: `hal.inria.fr:inria-00595460`.

[35] Lawrence Shampine and Mark Reichelt. "The Matlab ODE Suite". *SIAM Journal on Scientific Computing* 18 (1997), 1–22.
DOI: `10.1137/S1064827594276424`.

[36] Clay Shonkwiler. *Principal angles in terms of inner products*. Technical report. University of Pennsylvania, 2009.

[37] Gilbert Strang and Truong Nguyen. *Wavelets and filter banks*. Wellesley: Wellesley-Cambridge Press, 1996.
ISBN: 0961408871.

[38] Christian Studer. *Numerics of unilateral contacts and friction. Modeling and numerical time integration in non-smooth dynamics*. Volume 47. Lecture Notes in Applied and Computational Mechanics. Springer, 2009.
ISBN: 3642010997.
DOI: `10.1007/978-3-642-01100-9`.

[39] Jhy-Horng Wang and W. K. Chen. "Investigation of the vibration of a blade with friction damper by HBM". *Journal of Engineering for Gas Turbines and Power* 115.2 (1993), 294–299.
DOI: `10.1115/1.2906708`.

[40] Yu Wang. "Dynamics of unsymmetric piecewise-linear/non-linear systems using finite elements in time". *Journal of Sound and Vibration* 185.1 (1995), 155–170.
DOI: `10.1006/jsvi.1994.0369`.

[41] John Williams and Kevin Amaratunga. "Introduction to wavelets in engineering". *International Journal for Numerical Methods in Engineering* 37.14 (1994), 2365–2388.
DOI: `10.1002/nme.1620371403`.

[42] Peter Wriggers. *Computational Contact Mechanics*. 2nd edition. Springer, 2006. ISBN: 3540326081.